3.5 SCCMS Projects

First-Principles Phase Field Mapping I

Kaoru Ohno

Department of Physics, Faculty of Engineering Science,

Yokohama National University, Tokiwadai, Hodogaya-ku, Yokohama 240-8501

To perform, for example, accurate mapping of first-principles results to phase field models, it would be necessary to perform accurate and reliable first-principles calculations. To analyze XPS spectra, the so-called ΔSCF method using MRDCI, CCSD, and other quantum chemistry approaches is applicable for isolated molecules, but the ΔSCF method using density functional theory (DFT) is generally not applicable to this problem in particular for crystals. So, relying on quasiparticle theory for a deep core hole, we performed GW calculation for XPS spectra of crystals using TOMBO [1]. The result is listed in Figure 1. On the other hand, a photoabsorbed excited state can be constructed by adding one electron to the second empty level of a cationic state. The neutral ground state is constructed by adding one electron to the first empty level of a cationic state. Then, the photoabsorption energy can be evaluated as a difference between these two energy gains in the two processes of adding an electron to a cationic state that can be simultaneously obtained by applying the GW(Γ) method to a cationic system without solving the Bethe-Salpeter equation. We called this method the GW(Γ) method without the Bethe-Salpeter equation. We succeeded in reproducing the experimental photoabsorption energy within the 0.1 eV accuracy by applying the self-consistent GWΓ method of TOMBO to several cationic systems as shown in Figure 2 [2].

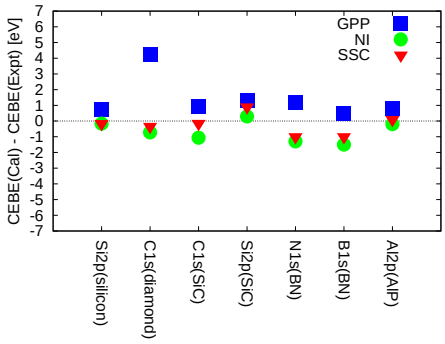

Fig. 1 Core electron binding energy (CEBE) difference between GW and experimental data.

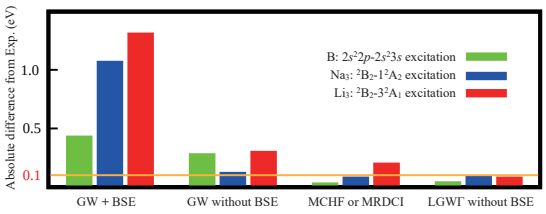

Fig. 2 Absolute difference of calculated photoabsorption energies from experimental data.

References

[1] Tsubasa Aoki and Kaoru Ohno, J. Phys.: Condensed Mat. (Letter, open access) **30**, 21LT01 (2018).

[2] Tomoharu Isobe, Riichi Kuwahara, and Kaoru Ohno, Phys. Rev. A **97**, 060502(R);1-6 (2018).

First-Principles Phase Field Mapping II

Kaoru Ohno

Department of Physics, Faculty of Engineering Science,

Yokohama National University, Tokiwadai, Hodogaya-ku, Yokohama 240-8501

Theoretical understanding of microstructure is very important in predicting the durability and performance of alloys. For this purpose, phase field models have been widely used to simulate the time evolution of microstructures and various properties. However, the results strongly depend on the input parameters, which are mostly empirical. Therefore, we propose a new and simple method to determine the input parameters purely from first principles. We developed first-principles phase field model by using cluster expansion theory and potential renormalization theory [1] together and succeeded in obtained an excellent result for Ni-Al alloy systems [2]. Our results clearly distinguish the local composition of alloys in accord with the experimental phase diagram (Fig 1). We have also succeeded in predicting the time evolution of microstructures of Ni-Al alloys at different compositions at 1300K.

References

[1] Y. Misumi, S. Masatsuji, R. Sahara, S. Ishii, and K. Ohno, J. Chem. Phys. **128**, 234702 (2008).

[2] S. Bhattacharyya, R. Sahara and K. Ohno, in submission to Nature Communications.

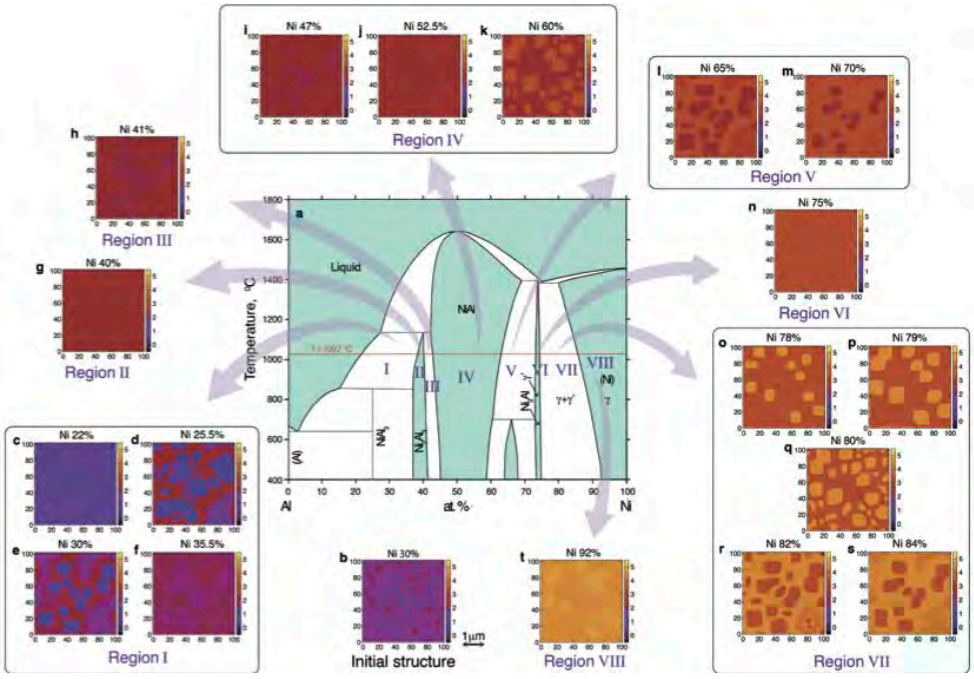

Fig. 1 Microstructures of NiAl alloys obtained by the first-principles phase field model

Electrochemical reaction on a platinum surface

OSAMU SUGINO

Institute for Solid State Physics,

The University of Tokyo, Kashiwa-no-ha, Kashiwa, Chiba 277-8581

The fuel-cell reactions can be recognized as a transfer of proton onto the reaction intermediates, O_2, O_2H, OH, H and O, adsorbed on the surface or a direct transfer onto the surface, but there still remain controversies even on the well-defined Pt(111) surface. While, the conventional approaches like density functional theory (DFT) within the generalized gradient approximation (GGA) for the exchange-correlation (xc) of electrons is not accurate enough to reveal all the details. In this context, we applied the random phase approximation (RPA) to investigate the H adsorption [1]. The calculated adsorption energy is 290 meV in consistent with experimentally estimated value $\leq$270 meV at full coverage condition although the GGA provides a value larger than RPA by 100 meV without the van der Waals (vdW) correction and a value larger by 30-40 meV with the correction. The most stable adsorption site is the fcc site although the top site is less stable only by 23 meV being comparable to the thermal energy at room temperature. The small difference in the adsorption energy indicates that H at the fcc site, H_{fcc}, coexists with H_{atop}, which explains why signal from the top site is measured experimentally, although GGA predicts predominance of H_{fcc}. The difference between RPA and GGA can be traced back to overestimation of the GGA on the lattice constant of Pt; interestingly, the relative adsorption energy, $\Delta E_{\mathrm{ads}} \equiv E_{\mathrm{ads}}(\mathrm{H_{fcc}}) - E_{\mathrm{ads}}(\mathrm{H_{atop}})$, happens to be similar between RPA and GGA when using a common lattice constant. Importantly, H_{fcc} is more stable than H_{atop} in RPA because the quantum confinement effect is much larger for H_{atop}: Within the classical approximation, H_{fcc} is less stable. The reversed order of stability suggests different proton transfer mechanism to occur between the quantum and classical systems; this may explain why the reaction efficiency is different between hydrogen and deuterium as observed experimentally. Further, our subsequent and preliminary simulations have shown that the solvent effect yields rather minor effect on the adsorption energies and the coverage effect is also minor; however, the adsorbed H can easily hop among fcc, hcp, and top sites when simulated at room temperature at a 2/3 coverage condition. The result suggests

incorrectness of the old picture that H_{fcc} plays a role as a spectator in the hydrogen evolution/oxidation reaction as if forming a stable hydrated structure. The result suggests a new picture, instead, that there is large fluctuation in the hydrogen density profile and fluctuation is associated with the enhancement of the reaction: Further investigation is admittedly needed to confirm this picture, which is remained as a target of the next-year project.

References

[1] L. Yan, Y. Sun, Y. Yamamoto, S. Kasamatsu, I. Hamada, and O. Sugino: J. Chem. Phys. **149** (2018) 167402.

Large-scale molecular simulation of two-dimensional glass-forming liquid

Hayato SHIBA
Institute for Materials Research, Tohoku University
2-1-1 Katahira, Aoba-ku, Sendai 980-8577

Recently, large-scale molecular dynamics simulation by the present author a and colloidal experiments have revealed that a two-dimensional (2D) liquid supercooled toward the glass transition exhibits long-wavelength phonon fluctuations that has been overlooked in the literature on glasses. These phonon fluctuations are stabilized by the rigidities emerging with decreasing temperatures, in a manner similar to those in 2D crystalline solids. Furthermore, its structural relaxation turns out to be similar between two and three dimensions, if structural changes in terms of neighbor switching is properly taken into account in considering the relaxation.

For this year, we have numerically investigated the the mechanism of the slowdown in the dynamics of a 2D supercooled liquid at a high number density $N/V = 1.2$, where the pairwise interactions are defined by a modified Kob-Andersen parameters Up to 4096000 particles are simulated using our original simulation codes optimally parallelized for the ISSP system. First, by investigating the diffusivity in the long-time limit, we have clarified that not only the long-wavelength phonons but also long-wavelength hydrodynamic flow affects the transport behavior in the present 2D liquid, causing logarithmically divergent diffusivity D in the long-time limit. We have carried out an explicit calculation of the velocity autocorrelation function a relatively high temperature $T = 1.0$ It exhibits coming and going between positive and negative correlations, and finally, in a system with millions of particles, pure hydrodynamic correlation turns out to emerge in the long-time limit.

We have also investigated the relaxation times τ_α, $\tau_{\rm R}$, and $\tau_{\rm B}$ defined as decay times of the following three relaxation functions: (a) The standard intermediate scattering function (ISF), density correlation defined on the basis of particle displacements, where fluctuations on the scale of particle sizes are considered. (b) Another ISF, representing local density fluctuation, defined on the basis of relative displacements between neighboring particles, and (c) The decay in the number of neighboring particles (*i.e.* imaginary "bonds"). We have compared these time scales with the stress relaxation in terms of the autocorrelation function $G(t) = (V/k_{\rm B}T)\langle\sigma_{xy}(t)\sigma_{xy}(0)\rangle$ with $\sigma_{xy}(t)$ the shear component of the stress tensor. In usual (three-dimensional) supercooled liquid, a proportionality $\tau_\alpha \sim \eta/T$ usually hold, but this relation breaks down in the 2D glass-forming liquids. Instead, an alternative proportionality $\tau_{\rm R} \sim \eta/T$ is found to hold by our careful calculation. This result suggests that the local density fluctuation governs divergence of viscosity with vitrification, behind elastic and hydrodynamic anomalies taking at long-wavelengths in 2D liquids.

References

[1] H. Shiba, T. Kawasaki, and K. Kim: in preparation.

Study of many-body correlation effects on spin relaxation rate in quantum dots

Kazuyoshi Yoshimi and Takeo Kato
Institute for Solid State Physics, University of Tokyo
Kashiwa-no-ha, Kashiwa, Chiba 277-8581

Quantum dot systems have been studied for long time to realize quantum devices utilizing microscopic quantum levels in analogy of the atoms. Using this property, it is utilized in a wide range of applications, such as quantum computer elements, optical non-linear switching, fluorescent probes in living organisms and solar cells. For these applications, the spin relaxation rate is one of the important parameters, which can be evaluated from accurate evaluation of the electronic state, which incorporate the effects of electron correlation, spin-orbit interaction, and electron-phonon coupling.

The calculation of spin relaxation rate is performed on a model with the confined-harmonic potential, electron-electron and spin-orbit interactions using the Fermi's golden rule[1]. Recently, we have developed a spin relaxation rate analysis tool for quantum dot systems using the quantum lattice model solver $\mathcal{H}\Phi$[2]. In this report, we introduce the tool through the actual calculation.

The Hamiltonian under the magnetic field B is given by[1]

$$\mathcal{H} = \mathcal{H}_0 + \mathcal{H}_{ee} + \mathcal{H}^R_{so} + \mathcal{H}^D_{so}. \quad (1)$$

Here, $\mathcal{H}_0 = \sum_i (\boldsymbol{P}_i^2/2m^* + (m^*\omega_0^2/2)r_i^2 + g\mu_B B\sigma_i^z/2)$ is the non-interaction part of the Hamiltonian, where $\boldsymbol{P}_i = -i\hbar\nabla_i + (e/c)\boldsymbol{A}_i$ with $\boldsymbol{A}_i = (B/2)(-y_i, x_i, 0)$ stands for the electron momentum, $\boldsymbol{r}_i$ is the position vector, and σ_i^l is the $l(=x,y,z)$-component of the Pauli spin matrices at i-th particle, respectively. m^* is the effective mass, ω_0 is the eigenfrequency of the confined-harmonic potential, g is the Lande's g factor, μ_B is the Bohr magneton and B is the magnetic field. $\mathcal{H}_{ee} = (e^2/2\kappa)\sum_{i\neq j} r_{ij}^{-1}$ is the electron-electron interaction part of the Hamiltonian, where κ is the static relative dielectric constant and r_{ij} is the distance between i-th and j-th particles. $\mathcal{H}^R_{so} = \sum_i(\alpha/\hbar)(P_i^y\sigma_i^z - P_i^x\sigma_i^y)$ and $\mathcal{H}^D_{so} = \sum_i(\beta/\hbar)(P_i^y\sigma_i^y - P_i^x\sigma_i^x)$ are the Rashba- and Dresselhaus-type spin orbit interactions part of the Hamiltonian with coupling constants α and β, respectively.

The spin relaxation rate is obtained by

$$\Gamma = \frac{2\pi}{\hbar}\sum_{\boldsymbol{q},\lambda}|M_{\boldsymbol{q},\lambda}|^2|\langle f|e^{i\boldsymbol{q}\cdot\boldsymbol{r}}|i\rangle|^2\delta(\epsilon_f-\epsilon_i-\hbar\omega_{\boldsymbol{q},\lambda}), \quad (2)$$

where $M_{\boldsymbol{q},\lambda}$ is the scattering matrix element, $\omega_{\boldsymbol{q},\lambda}$ is the phonon energy spectrum of branch λ and momentum $\boldsymbol{q}$, respectively. $\epsilon_{i(f)}$ is the energy at the initial (final) state. In our calculation, we use the long wavelength approximation $|M_{\boldsymbol{q},\lambda}|^2 \sim M_\lambda(\tilde{q})^2 g_\lambda(\theta,\phi)$. The three types of electron-acoustic phonon scatterings are considered. One is the scattering due to the deformation potential, $M_\lambda(\tilde{q})^2 = (\hbar\Xi^2/2DVv_{sl}l)\tilde{q}_l$, $g_{sl}(\theta,\phi) = 1$, where D is the crystal density, Ξ is the acoustic deformation potential constant, v_{sl} is the sound speed for longitudinal phonon mode, l is the magnetic length and $\tilde{q} = ql$ is the dimensionless parameter. The second is the scatterings due to the piezoelectric field for the longitudinal phonon mode, $M_{pl}(\tilde{q})^2 = (32\pi^2\hbar e^2 e_{14}^2 l/\kappa^2 DVv_{sl})/\bar{q}_l$, $g_{pl}(\theta,\phi) = 9\sin^4\theta\cos^2\theta\sin^2\phi\cos^2\phi$, where

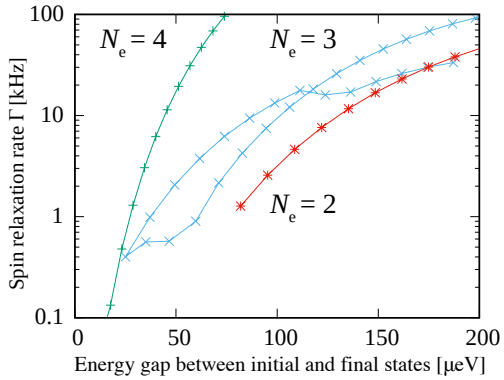

Figure 1: The energy-gap between initial and final states dependency of the spin-relaxation rates from the high spin state to the low spin state at $N_e = 2, 3, 4$.

e_{14} is the piezoelectric constant. The other is the piezoelectric field for the transverse phonon mode, $M_{pt}(\tilde{q})^2 = (32\pi^2\hbar e^2 e_{14}^2 l/\kappa^2 DV v_{st})/\tilde{q}_l$, $g_{pl}(\theta,\phi) = \sin^2\theta\cos^2\theta + \sin^4\theta\cos^2\phi\sin^2\phi - 9\sin^4\theta\cos^2\theta\sin^2\phi\cos^2\phi$, where v_{st} is the sound speeds for transversal phonon mode.

To analyze the quantum dot system, we first consider the eigenstates of the one-body part Hamiltonian. By mapping the basis of $\mathcal{H}_{ee}$ into these states and using the configuration interaction method, we obtain the eigenstates of $\mathcal{H}$ using numerical exact diagonalization method. In this calculation, we consider the 28 basis. The parameters are set as follows; $\hbar\omega_0 = 2.65$ [meV], $m^* = 0.067, \kappa\epsilon_0 = 12.9, g = -0.28, \alpha = 0$, $\beta = 25$ [meVÅ], $D = 5.31\times10^3$ [kg/m^3], $v_{sl} = 4.72\times10^3$ [m/s], $v_{st} = 3.34\times10^3$ [m/s], $e_{14} = 1.41\times10^9$ [V/m], $\Xi = 8.6$ [eV]. The magnetic field B is varied from 1.5 to 2.5[T]. In Fig. 1, the spin relaxation rates from the high spin state to the low spin state at the electron number $N_e = 2, 3, 4$ are shown. We found that the energy-gap dependence of spin relaxation rates shows the similar behavior of the experiments, i.e. the spin relaxation rates become large with increasing N_e in the small energy-gap region[3].

Finally, parallelization performance using GPGPU calculation is briefly described. Since $\mathcal{H}_{ee}$ is mapped into the basis of the one-body part of the Hamiltonian, the total numbers of the Coulomb interactions becomes about $(2N_s)^4$, where N_s is the total number of considered basis. When the electron number is a few, the Hilbert space becomes small and thus the parallelization about interaction terms is efficient. For comparison, we calculated the ground state on the 28 basis Hubbard model at 5 electrons by the hybrid parallelization with 72 processes and 12 threads (MPI+OpenMP) and 2 GPUs (MPI+GPGPU), respectively. We found that the latter calculation becomes 4 times faster than the former calculation. Thus, the GPGPU implementation is expected to be useful for searching the suitable parameters in the quantum dot systems. Our tools are still under development and thus not yet released. However, we plan to release it as free-software after some improvements.

Acknowledgement: We thank A. Oiwa, H. Kiyama, and T. Misawa for fruitful discussions. This work was supported by support service of program portability to General Purpose Graphics Processing Unit. Numerical calculations were mainly performed at the Supercomputer Center, Institute for Solid State Physics, University of Tokyo.

References

[1] M. Rontani, C. Cavazzoni, D. Bellucci et al., J. Chem. Phys. 124 124102 (2006); J. I. Climente, A. Bertoni, G. Goldoni et al. Phys. Rev. B 76 085305 (2007).

[2] M. Kawamura, K. Yoshimi, T. Misawa, Y. Yamaji, S. Todo, N. Kawashima, Com. Phys. Comm. **217**, 180 (2017).

[3] H. Kiyama and A. Oiwa (Private communication).

Unified Photonic-Electronic Devices

Kazuhiro YABANA

Center for Computational Sciences,

University of Tsukuba, Tsukuba 305-8577

We develop a first-principles computational method to investigate electron dynamics induced by ultrashort laser pulses based on time-dependent density functional theory (TDDFT) in real time. We develop the code SALMON (Scalable Ab-initio Light-Matter simulator for Optics and Nanoscience) and make it open to the public at our website, http://salmon-tddft.jp. The code paper of SALMON has been published recently [1].

SALMON has been developed so that it runs efficiently in supercomputers with various kinds of professors. To make a comparison of performance with the processor Xeon Gold 6148 of Skylate-SP architecture equipped in System C, we use the System C to obtain the performance data. SALMON has already been optimized for many-core processors such as Knights Landing Xeon Phi 7250 that is equipped in Oakforest-PACS at JCAHPC. Since Skylate-SP architecture is quite close to the many-core, we confirmed that the present version of SALMON runs efficiently at System C without further efforts, with performance about 40% relative to the theoretical one.

As a new feature of SALMON, we have developed a theory and computational method to describe interaction of strong and ultrashort pulsed light with thin materials, from atomic monolayer to thick films. The method solves the time-dependent Kohn-Sham equation and the Maxwell equations using a common spatial grid. We have also developed a two-dimensional (2D) theory describing optical responses of thin materials in TDDFT, without the elaborate coupling with Maxwell equations. It was found that the latter 2D theory is justified for films of thickness less than 5nm for Si nano-films through the comparison with the former elaborate calculation.

References

[1] M. Noda, S.A. Sato, Y. Hirokawa, M. Uemoto, T. Takeuchi, S. Yamada, A. Yamada, Y Shinohara, M. Yamaguchi, K. Iida, I. Floss, T. Otobe, K.-M. Lee, K. Ishimura, T. Boku, G.F. Bertsch, K. Nobusada, K. Yabana, “SALMON: Scalable Ab-initio Light–Matter simulator for Optics and Nanoscience”, Comp. Phys. Comm. 235, 356 (2019).

Ring Decomposition of Tensors[1]

Naoki KAWASHIMA
Institute for Solid State Physics, University of Tokyo
Kashiwa-no-ha, Kashiwa, Chiba 277-8581

While the tensor-network-based methods for renormalization group (TNRG) are similar to the Migdal-Kadanoff RG in essense, they generally provides much more accurate and, more importantly, systematic and controllable series of approximations. Theoretically, the approximation made there becomes infinitly accurate as we increase the bond-dimension, the control parameter of the methods. However, in practice, it is not so easy. One of the main sources of difficulty is the contributions from short-range correlations. While there are a few proposals for removing these undesirable contributions, separation of such contribution from the fixed-point tensors is usually a non-linear optimization problem and, therefore, may take a long time to find the optimal solution. Meanwhile, the tensor-ring decomposition of tensors plays a key role in various applications of tensor network representation in physics as well as in other fields. In most heuristic algorithms for the tensor-ring decomposition, one encounters the problem of local-minima trapping. This is essentially the same problem as we encounter in the TNRG. Particularly, the minima related to the topological structure in the correlation are hard to escape. Therefore, identification of the correlation structure, somewhat analogous to finding matching ends of entangled strings, is the task of central importance. We propose [1] a method for solving this problem.

For a bench-mark test, we consider a corner-double-line (CDL) tensor. The CDL tensor appears typically in the TNRG as a part of renormalized tensors. It represents the short-range component of the correlations. Specifically, we consider the 3rd-order CDL that consists of three 9-dimensional outher indices and three 3-dimensional inner indices as illustrated in the inset of the figure. We apply our method for varying dimensions for the inner indices, and compare the results with the alternating-least-square method. The contrast is very clear.

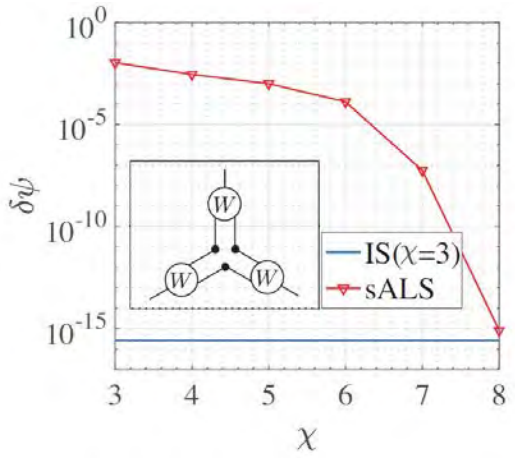

Figure 1: The comparison of the approximation errors $\delta\psi$ obtained by the present method and a heuristic method (sALS) as a function of the bond dimension χ. The target tensors are a third-order corner-double-line tensor with the dimension of the inner bonds fixed to be 3. (Adopted from [1])

[1] This report is based on Hyun-Yong Lee and Naoki Kawashima (arXiv:1807.03862).

Simulation of organic-inorganic interfaces

Shuji OGATA
Nagoya Institute of Technology
Gokiso-cho, Showa-ku, Nagoya 466-8555, Japan

In the fiscal year of 2018, we have addressed two subjects using our, hybrid quantum-classical (QM-CL) simulation code and classical MD code.

Subject 1: Chemical Reactions Involved in Moisture-Induced Weakening of Adhesion Between Aluminum and Epoxy Resin [1]. Using the hybrid QM-CL simulation method, we have successfully reproduced the adhesion strengths between surface-oxidized Al and bisphenol-A (bisA) resin at a comparative magnitude to the experimental values. For the DFT calculation of the QM region, the divide-and-conquer- type real-space grid code (DC-RGDFT) is used with the PBE-GGA xc-potential and the norm-conserving pseudopotentials. We divide the QM region with the buffer Al atoms and set the grid points with size h = 0.2911 Å to represent the eigenfunctions and potentials; finer grid points are auxiliarily set around C and O atoms. The h corresponds to the cutoff energy 3.81 $(\pi/\mathrm{h(Å)})^2$ = 443 eV in the plane-wave representation. The nine-point finite difference method is adopted to calculate their derivatives.

As the water content in the contact region has increased (case A < case B < case C), the calculated adhesion strength has decreased in the ordering of case B > case A > case C. In cases A and B, where a liquid layer has not been formed in the contact region, we have found that some of the OH groups of the bisA molecules reacted with surface Al atoms. In case C, the surface Al atoms have been well saturated by OH and H_2O molecules and the liquid layer in the contact region has been alkaline. Some of the bisA ether groups have been broken due to the alkaline environment.

We compare cases A-C in the present study with the experimental conditions. In case A, the surface oxide had no H atom; therefore, it was reactive with the bisA OH group. In case B, all the H_2O molecules in the contact region reacted with the surface oxide. The surface oxide in case B still reacted with the bisA OH group. An alkaline (free OH-rich) liquid layer was formed in case C. Under experimental conditions, the theoretical alkaline liquid layer may become neutralized through other environmental factors unaccounted for by the computation, e.g., the experimental deformation speed is much slower than the present value and hence free OH may diffuse to environment. Therefore, the experimentally dry conditions correspond best to either case B or intermediate between cases B and C. The wet condition corresponds to case C.

Subject 2: Novel Calculation Scheme for the Work of Adhesion between a Liquid and Polymer-Grafted Substrates [2]. A method to calculate the work of adhesion appropriate for the interface between a liquid and a polymer-grafted solid surface was developed herein by using two novel ideas. First, spherically symmetric potentials were introduced to separate the liquid molecules from the solid surface according to its shape. Second, a parameter update scheme for the potentials was defined so that sharp variations in the free energy gradient are suppressed when the liquid molecules are separated gradually from the solid surface. The proposed method was applied at the interface between water and a gold substrate modified by poly(ethylene oxide).

References

[1] S. Ogata and M. Uranagase, J. Phys. Chem. C **122** (2018) 17748-17755.
[2] M. Uranagase, S. Ogata, et al., J, Phys. Chem. Phys. **148** (2018) 064703-1-9..

Conversion and storage of energy−fuel cells and secondary batteries: Research and development of fundamental technologies of battery simulators.

Susumu OKAZAKI
Department of Materials Chmistry, Nagoya University
Furo-cho, Chikusa-ku, Nagoya 464-8603

The goal of our project is to develop the basic technology of the whole battery simulator. One of the key techniques is molecular-level design of polymer membranes controlling transportation of protons and ions across the membrane with proper stiffness resistant to mechanical deformation under external stress. Such membranes are widely applicable to the fuel cells used in the industrial products.

On the system B and C, we performed fully atomistic molecular dynamics (MD) calculations of hydrated perfluorosulfonic acid (PFSA) ionomers composed of a hydrophobic polytetrafluoroethylene backbone with hydrophilic side chains terminated by sulfonic acid[1], as a model of proton exchange polymer electrolyte membrane of fuel cells. On the basis of these atomistic MD calculations, we constructed a predictive coarse-grained (CG) model for the structure and morphology of PFSA membranes[2]. A series of molecular dynamics simulations of PFSA ionomers with different side chain (SC) length explored the effect of SC length on the morphology and mechanical properties of the PFSA membrane[3]. To realize a tensile test of polymer materials, microscopic expression of the pressure tensor using the fast multipole method (FMM) with periodic boundary conditions are derived[4].

These results will contribute to the development of higher performance fuel−cells and secondary batteries and to the realization of the entire battery simulator in the near future.

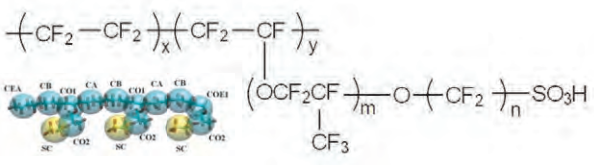

Figure 1: Molecular structure of perfluorosulfonic acid (PFSA) ionomers. Inserted figure is the CG model of PFSA ionomers[2].

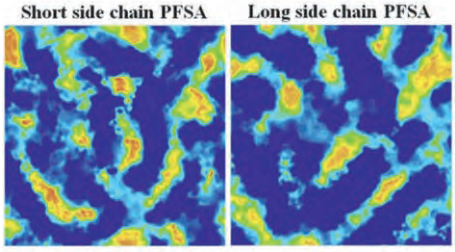

Figure 2: Number density maps of sulfonic acid groups, water, and hydronium ions at one cut plane for PFSA ionomers with different side chain length[3].

References

[1] A. T. Kuo, W. Shinoda, S. Okazaki : J. Phys. Chem. C **120** (2016) 25832.

[2] A. T. Kuo, S. Okazaki, W. Shinoda : J. Chem. Phys. **147** (2017) 094904.

[3] A. T. Kuo, K. Takeuchi, A. Tanaka, S. Urata, S. Okazaki, and W. Shinoda : Polymer **146** (2018) 53.

[4] N. Yoshii, Y. Andoh, S. Okazaki : J. Comput. Chem. **39** (2018) 1192.

Development of an excited-state theory based on many-body Green's functions and fragment molecular orbital method

Takatoshi Fujita
Institute for Molecular Science
Myodaiji, Okazaki, Aichi 444-8585

Predicting charge-transfer (CT) excited states across the donor/acceptor interface is essential for understanding the charge photogeneration process in an organic solar cell. However, the first-principles computations of the CT states in an organic/organic interface remain challenging, because both electron correlation and polarizable environmental effects must be taken into account. The GW many-body Green's function theory [1] can offer an accurate and practical scheme to explore electronic states in condensed matter. The quasiparticle energy directly corresponds to a charged excitation energy, such as an ionization potential or an electron affinity. The neutral excitation energy can also be computed in combination with the Bethe-Salpeter equation (BSE). Although the recent developments of the computational algorithm have enabled a GW calculation for a system over 100 atoms, it is still difficult to treat very large system over 1,000 atoms.

To extend the applicability of GW to larger and more complex systems, we have been developing the large-scale GW method based on the fragment molecular orbital (FMO) method [2]. The total polarization function is approximated as the sum of intrafragment polarization functions that are calculated from fragment molecular orbitals in the FMO method. The combined GW and COHSEX approximations is employed to calculate self-energies, in which the dynamically-screened Coulomb potential is explicitly evaluated for a target fragment, while the statistically-screened Coulomb potential of the entire system is evaluated at the COHSEX level. Based on the fragment-based implementation, we have performed a large-scale GW calculation for an organic/organic interface system over 2,000 atoms. We have highlighted the effects of the environmental polarization effects on the CT states. The FMO-based formalism can be applied to any disordered or heterogeneous molecular aggregates for the accurate evaluation of charged excitations and also provides a starting point for the optical excitations within the BSE. In combination with the fragment-based excited-state theory [3, 4], the delocalized excited states can also be treated.

References

[1] L. Hedin, Phys. Rev. **139** (1965) A796.

[2] T. Fujita, Y. Noguchi, Phys. Rev. B **98** (2018) 205140.

[3] T. Fujita, Y. Mochizuki, J. Phys. Chem. A **11** (2018) 3886.

[4] T. Fujita, A. M. Khorshed, T. Hoshi, **20** (2018) 26443.

First-principles materials design by multi-scale simulation

Tetsuya FUKUSHIMA
Institute for NanoScience Design, Osaka University, Osaka 560-8531, Japan
Institute for Datability Science, Osaka University, Osaka 565-0871, Japan

A "scale-bridging" (multi-scale) simulation technique, combining the Korringa-Kohn-Rostoker (KKR) Green's function method and model approaches, was developed this year. On the basis of the "scale-bridging" simulation technique and massively parallel computing, we designed new functional dilute magnetic semiconductors (DMSs), such as Fe-based DMSs [1] and Eu-based DMSs [2]. Here, we introduce the materials design of the Fe-based DMS systems.

Fe-based DMSs have recently been attracting much attention. In particular, in Fe-doped III-V semiconductors, the substitutional Fe atoms are expected to exist as a neutral state (Fe^{3+}), in which case they will not provide extrinsic carriers for the system. Thus, the conduction carriers are not provided by the doped Fe impurities but instead are supplied from the conduction or valence bands. Since the effect of impurity scattering is small, the coherence length is increased. This provides the possibility of realizing new functionalities, such as low power consumption and high-speed operation, due to the quantization of the electronic structures. It is also noteworthy that both n- and p-type DMS systems can be fabricated easily since the carrier characteristics can be controlled independently of the Fe impurities.

We have elucidated the effects of n- and p-type doping and of the Fe distribution on the magnetic properties of DMSs and have investigated the possibility of high $T_{\rm C}$. For this purpose, we have demonstrated the control of the magnetic exchange coupling constants (J_{ij}), chemical pair interactions (V_{ij}), and T_C in (Ga,Fe)Sb and (In,Fe)Sb by changing the carrier characteristics (i.e., chemical potential), using first-principles electronic structure calculations. J_{ij} is calculated by the Liechtenstein's formula:

$$J_{ij} = \frac{1}{4\pi}\mathrm{Im}\int^{E_{\rm F}} dE\ \mathrm{Tr}_L\{\Delta_i T_{\uparrow}^{ij}\Delta_j T_{\downarrow}^{ij}\}, \quad (1)$$

where $\Delta_i = t_{i\uparrow}^{-1} - t_{i\downarrow}^{-1}$, with $t_{i\uparrow(\downarrow)}$ being the atomic t-matrix of the magnetic impurities at site i for spin up (down) state. $T_{\uparrow(\downarrow)}^{ij}$ is scattering path operator between site i and j for spin up (down) state. Tr_L is the trace over the orbital variables. We calculate V_{ij} by the generalized perturbation method expressed as

$$V_{ij} = -\frac{1}{\pi}\mathrm{Im}\int^{E_{\rm F}} dE\ \mathrm{Tr}_L\{\Delta T_{\uparrow}^{ij}\Delta T_{\downarrow}^{ij}\}, \quad (2)$$

where $\Delta = t_{\rm A}^{-1} - t_{\rm B}^{-1}$, with $t_{\rm A(B)}^{-1}$ being the atomic t-matrix of the A(B) atom. The Liechtenstein's formula and generalized perturbation method make it possible to calculate Fermi level dependence of J_{ij} and V_{ij} by replacing the Fermi level $E_{\rm F}$ with a variable energy. Finally, $T_{\rm C}$ is estimated by the random phase approximation, which is based on the Tyablikov decoupling method.

The results from our KKR Green's function calculations clearly indicate that isoelectronic Fe dopants induce antiferromagnetic interactions due to the superexchange mechanism in both GaSb and InSb. By considering artificial changes in the Fermi level, we

have found that the magnetic exchange coupling constants in these systems exhibit universal behavior. Antiferromagnetic-ferromagnetic transitions occur for both n- and p-type doping, and this behavior can be well understood in terms of the Alexander-Anderson-Moriya mechanism. The Fermi level dependence of the chemical pair interactions also shows characteristic features, which can be reasonably explained by magnetic frustration and the nature of the covalent bond. Our multi-scale simulations show that finite values of T_{C} are realized in n- and p-type regions. For p-type doping, the spinodal nano-decomposition caused by annealing drastically enhances T_{C}. However, for n-type doping, the initial phases have higher T_{C} values than the final phases. Based on the results of our calculations, we propose that high values of T_{C} may be realized and that the magnetic states of (Ga, Fe)Sb and (In, Fe)Sb may be manipulated by controlling the gate voltage, chemical doping, and annealing process. Such features will be very important for next-generation semiconductor spintronics.

References

[1] H. Shinya, T. Fukushima, A. Masago, K. Sato, and H. Katayama-Yoshida, J. Appl. Phys. **124** (2018) 103962.

[2] A. Masago, H. Shinya, T. Fukushima, K. Sato, and H. Katayama-Yoshida, Phys. Rev. B **98** (2018) 214426.

Electron Theory on Sodium Secondary-Battery Materials

Hiroki KOTAKA[1], Motoyuki HAMAGUCHI[2], Hiroyoshi MOMIDA[1,2], Tamio OGUCHI[1,2]
[1]*ESICB, Kyoto University, Katsuragoryo, Kyoto, Kyoto 615-8245*
[2]*ISIR, Osaka University, Mihogaoka, Ibaraki, Osaka 567-0047*

Microscopic mechanism of charge/discharge reactions in several battery systems is studied by first-principles calculations to explore new sodium secondary batteries. In this year, we focus on Na/SnS and Li/Li$_x$$MTiO_4$ (M=V, Mn, Fe, Co, and Ni) systems.

Tin compounds are known as high-capacity materials in charge/discharge reactions and have advantages in price and safety for practical applications, being considered as a good candidate for the anode materials of sodium secondary battery.[1, 2] We investigate the electronic mechanism in discharge reactions in Na/SnS system. From experimental works, several stages are involved in conversion reactions starting from SnS. We clarify the possible reaction route considering the intermediate process of the discharge reaction, and theoretically obtain the reaction formulae of the Na/SnS battery systems. In SnS cathode, Na_4SnS_4, Sn, and Na_2S are generated as intermediate products. In addition, generated Sn and newly introduced Na may react to form several alloy phases as $NaSn_5$→$NaSn_2$→$NaSn$→Na_9Sn_4→$Na_{15}Sn_4$.
This multi-stage discharge reaction may explain discharge voltage-capacity curve measured by Kitajou *et al.*[3] To identify possible phases in the discharge reaction, calculated x-ray absorption spectroscopy (XAS) spectra for SnS and Na_2S are compared with experimental ones.[3] In order to accurately calculate the excitation energy, we perform the transition probability including the core hole effect. By the comparison of XAS spectrum, the intermediate phases Na_2S and Na_4SnS_4 are confirmed. The reaction products Na_2S and Na_4SnS_4 can precipitate in the SnS electrodes during the discharge process and the electrode is recovered to be SnS again after charging.

The so-called cation-disordered rock-salt materials including Li_2MnTiO_4 have attracted much attention because of a possible candidate for high-voltage and high-capacity cathode materials of Li-ion batteries. In this rock-salt-based oxides, high stability to O dissociation is highly expected because of the rigid and dense atomic structure. Recently, it has been experimentally reported that the battery performance such as capacity can be significantly improved by optimizing the Li composition ratio as to be $Li_{2+2x}Mn_{1-x}Ti_{1-x}O_4$ with the best value of $x \sim 0.2$. In this study, we perform the first-principles calculations for $Li_{2+2x}Mn_{1-x}Ti_{1-x}O_4$ models with several Li excess amount of x ranging from 0 to 0.5. Effects of x on the theoretical voltage-capacity profiles are compared with the experimental results. From the calculations, it is found that a two-stage process associated with Mn+Ti and Mn+O redox reactions take place depending on the Li concentration especially in the early and late discharge process, respectively.

References

[1] J. W. Wang *et al.*, Nano Lett. **12**, 5897 (2012).

[2] C. J. Pelliccione *et al.*, J. Phys. Chem. C **120**, 5331 (2016).

[3] A. Kitajou and S. Okada, private communications.

Development of permanent magnet materials

Takashi MIYAKE
CD-FMat, AIST
Umezono, Tsukuba, Ibaraki 305-8568

High performance permanent magnets require high saturation magnetization and high coercivity. The RFe$_{12}$-type compounds (R=rare-earth) having the ThMn$_{12}$ structure are potential main phase of high performance magnets, because they have high saturation magnetization and strong magnetoctystalline anisotropy for proper choice of R. The former comes from high Fe content, whereas the R element is essential for the latter. However, RFe$_{12}$ are thermodynamically unstable. We have studied stability of RFe$_{12}$ for a series of R element by means of density functional theory in the generalized gradient approximation. The R-4f electrons are treated as open-core states. Figure 1 shows the formation energy of RFe$_{12}$ relative to R_2Fe$_{17}$ and α-Fe [1]. We found that the stability is sensitive to the choice of R element. There is strong correlation between the atomic radius of the R element and the stability. The formation energy shows a minimum for R=Dy. It was reported recently that Sm(Fe,Co)$_{12}$ has excellent intrinsic magnetic properties. The present result indicates that partial substitution of Sm with e.g. Gd, Y and Zr would enhance the stability of the compound. We also calculated spin dispersion of Sm(Fe,Co)$_{12}$ from first-principles [2]. We found that the spin-wave dispersion of SmFe$_{12}$ is highly anisotropic around the Γ point. It is shown that the spin waves propagate more easily in the a^*-direction than in the c^*-direction. The spin-wave stiffness is enhanced by Co-doping.

We have been developing computational scheme for magnetization reversal using spin model for Nd$_2$Fe$_{14}$B. This year, we have developed a computational scheme for evaluating exchange stiffness constant by connecting analyses with two different scales of length, namely, Monte Carlo method for an atomistic spin model and Landau-Lifshitz-Gilbert equation for a continuous model. We found that the magnitude and temperature dependence of the exchange stiffness depends on the orientation in the crystal [3].

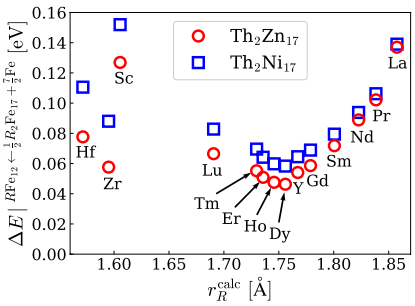

Figure 1: Formation energy of RFe$_{12}$ relative to R_2Fe$_{17}$ and α-Fe.

References

[1] Y. Harashima et al.: J. Appl. Phys. **124** (2018) 163902.

[2] T. Fukazawa et al.: J. Magn. Magn. Mater. **469** (2019) 296.

[3] Y. Toga et al.: Phys. Rev. B **98** (2018) 054418.

First-principles calculations of interface magnetic properties at magnetic materials

Yoshihiro GOHDA
Department of Materials Science and Engineering, Tokyo Institute of Technology
J1-3, Nagatsuta-cho 4259, Midori-ku, Yokohama 226-8502, Japan

Magnetic materials such as permanent magnets, multiferroic materials [1–3], and magnetic refrigerants are not only important in practical applications but also of significant interest fundamentally in the sense of understanding of magnetism due to electron-electron interaction. In such materials, effects of interfaces are significant: the coercivity of permanent magnets comes from interfaces in microstructures; a practical magnitude of multiferroicity is achievable only using the interface effects. However, our understanding of interface effects in magnetic materials is far from being complete. Furthermore, in the viewpoint of large scale computations, first-principles calculations of interfaces are challenging, because they are typically performed with large supercells.

In this project, first-principles studies were performed to understand magnetic materials, in particular permanent magnets [4–8] and multiferroic materials [3, 9]. First, on the basis of first-principles melt-quench molecular dynamics simulations by the OpenMX code [10], we performed structural analyses using graph theory for amorphous Nd-Fe alloys, a relevant subphase in Nd-Fe-B permanent magnets [5]. With improving the implementation of the Liechtenstein method in the OpenMX code, we also examined the exchange-coupling constants between two atoms in the Nd-Fe amorphous phase. We obtained strong composition dependence of the Curie temperature.

We also investigated the interface multiferroicity [3, 9]. The magnetoelectric coupling in a ferromagnetic/multiferroic interface, bcc-Fe/$BiFeO_3$(001), is significantly large [3]. We further clarified that the interface-magnetic anisotropy governs the direction of the bcc-Fe magnetization through the exchange coupling within bcc Fe. As for ferromagnetic/ferroelectric interfaces [9], we succeeded in enlarging interface magnetoelectric couplings by modifying the stacking of atomically controlled ferromagnetic thin-film heterostructures with Heusler alloys.

[1] T. Taniyama, J. Phys.: Condens. Matter **27**, 504001 (2015).

[2] C.-G. Duan, S. S. Jaswal, and E. Y. Tsymbal, Phys. Rev. Lett. **97**, 047201 (2006).

[3] K. Fujita and Y. Gohda, Phys. Rev. Appl. **11**, 024006 (2019).

[4] Y. Tatetsu, S. Tsuneyuki, and Y. Gohda, Mater. **4**, 388 (2018).

[5] A. Terasawa and Y. Gohda, J. Chem. Phys. **149**, 154502 (2018).

[6] Y. Tatetsu, Y. Harashima, T. Miyake, and Y. Gohda, Phys. Rev. Mater. **2**, 074410 (2018).

[7] N. Tsuji, H. Okazaki, W. Ueno, Y. Kotani, D. Billington, A. Yasui, S. Kawaguchi, K. Sugimoto, K. Toyoki, T. Fukagawa, T. Nishiuchi, Y. Gohda, S. Hirosawa, K. Hono, and T. Nakamura, Acta Mater. **154**, 25 (2018).

[8] Y. Gohda, Y. Tatetsu, and S. Tsuneyuki, Mater. Trans. **59**, 332 (2018).

[9] Y. Hamazaki and Y. Gohda, in preparation.

[10] T. Ozaki, Phys. Rev. B. **67**, 155108 (2003).

Multiscale simulations on complex multiphase flows

Yohei MORII, Takahiro MURASHIMA and Toshihiro KAWAKATSU

Department of Physics, Tohoku University, Sendai 980-8578

Multiphase flows, such as cavitation flows, flows in clouds, are complex flows where multiscale domain structures generated by phase coexistence play an important role in determining the macroscopic properties of the flow. Here, the main problem arises from the fact that the microscopic state at any point of the flow changes often in an unpredictable manner. This is due to the inhomogeneity of the flow, where a simple constitutive equation cannot be applied.

To solve such a problem, we develop Multi-Scale Simulation Platform for complex flows (MSSP), where microscopic simulators (MicS) such as molecular dynamics simulators are embedded in each point of the macroscopic flow (See Fig.1). We adopt Smoothed Particle Hydrodynamics (SPH) simulation technique, where the macroscopc flow is described by many hydrodynamic particles. In the MSSP, each hydrodynamic particle has one MicS as a representative of its microscopic state. We performed a benchmark simulation of MSSP on a macroscopic flow passing a cylindrical obstacle with use of Newtonian constitutive equation or Maxwell's constitutive equation as MicS. The results are shown in Fig.2. We also obtain quantitatively similar results to those in Fig.2 by using a set of many dumbbells as MicS. Simulation results show that the non-Markovian nature of viscoelastic fluid.

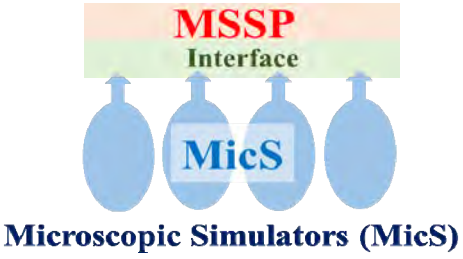

viscoelastic fluid.Fig. 1: Concept

As the correlation between MicS's arises only through the SPH level, the calculations of the time evolution of MicS's can be performed independently, which guarantees a high performance of parallelization calculation of MSSP.

Acknowledgements

This research was supported by MEXT, Japan as "Exploratory Challenge on Post-K computer" (Challenge of Basic Science – Exploring Extremes through Multi-Physics and Multi-Scale Simulations).

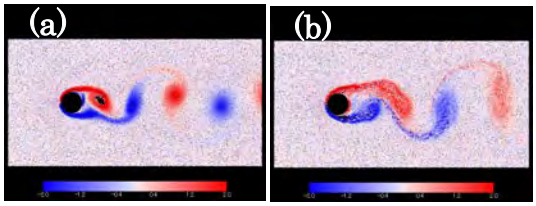

Fig. 2: (a) Newtonian fluid and (b)

Computational study of hydrous minerals using the path integral molecular dynamics method II

Tsutomu Kawatsu, and Toshiaki Iitaka

Computational engineering application unit, R&D group, Head office for information system and cybersecurity, Riken, 2-1 Hirosawa, Wako, Saitama 351-0198

We calculated thermodynamical structures of ice VIII-VII-X models [1] which was similar to the high-pressured hydrous mineral, δ-AlOOH [2,3] that we have calculated in last-year project. The δ-AlOOH has hydrogen bonds between polyhedrons of aluminium oxides, which symmetrize in high-pressured condition and asymmetrize in low pressure. The extremely high-pressured ices, ice X has symmetrized hydrogen bonds and relatively lower pressured ice VIII has asymmetrized ones. The ice VII is then a disordered intermediate state.

We used ab initio path integral molecular dynamics (AI-PIMD) method [4] with the parallel PIMD code [5] linked with parallel electronic structure calculation code, Quantum Espresso (QE) [6]. The AI-PIMD calculations in present study constructed in thirty-two parallel QE processes for the same number of connected replicas with single-node parallel of the QE process in system B. We then took 100,000 NPT sampling steps after 10,000 equilibrium steps for each trajectory and each pressure condition in every 10 GPa from 10 to 140 GPa. The temperature was set to 300 K. We used a minimum cell including two water molecules. The k-points was x3x3x3 and the energy cut off was 100. Ry.

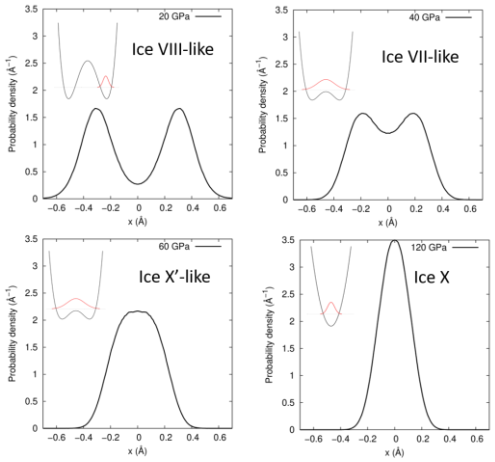

Fig. 1. Computed hydrogen-atom distributions between hydrogen-bonded water molecules in high pressures. The illustration in each graph is the overview of the potential and wave function of the hydrogen atom.

Figure 1 shows the computed distributions of the hydrogen atoms projected to the oxygen-oxygen axis using AI-PIMD method. These calculations represented the ice phases of VII, VIII, and X depending on the pressure. Using these structural distributions, we calculated quantum kinetic energy of the hydrogen and oxygen atoms. The kinetic energy of the hydrogen atom strongly depends on the phase of

the ice while that of the oxygen atom only depends on the pressure itself. On the other hand, δ-AlOOH has little different view. Instead of the hydrogen atom, the quantum kinetic energy of both the hydrogen and oxygen atoms are affected by the phase transition because the order of Al-O bonds can be changed with O-H bonds even though the oxygen atom is 16 times heavier than the hydrogen atom.

References

[1] E. Sugimura, T. Iitaka, K. Hirose, K. Kawamura, N. Sata, Y. Ohishi: Phys. Rev. B **77** (2008) 214103.

[2] A. Suzuki, E. Ohtani, T. Kamada: Phys. Chem. Minerals **27** (2000) 689.

[3] A. Sano-Fukukawa, H. Kagi, T. Nagai, S. Nakano, S. Fukura, D. Ushijima, R. Iizuka, E. Ohtani, T. Yagi: Am. Mineral. **94** (2009) 1255.

[4] G. J. Martyna, A. Hughes, M. Tuckerman: J. Chem. Phys. **110** (1999) 3275.

[5] S. Ruiz-Barragan, K. Ishimura, M. Shiga: Chem. Phys. Lett., **646** (2016) 130.

[6] P. Giannozzi *et al.*: J.Phys.: Condens. Matter 21 (2009) 395502.

Structure study of ε-solid oxygen using ab initio molecular dynamics

Tsutomu Kawatsu, Le The Anh, and Toshiaki Iitaka

Computational engineering application unit, R&D group, Head office for information system and cybersecurity, Riken, 2-1 Hirosawa, Wako, Saitama 351-0198

This study is a part of preliminary study for "structure study of silicate melts using linear scaling ab initio molecular dynamics." The silicate melts are an important component of the earth science, which is often called as "magma" if it is on the surface area of the earth. The magma is made in the deep earth and it forms various minerals depending the temperature and pressure. To calculate the silicate melts we have to optimize the computational methods which can describe the both crystal and molecular systems and calculate large system size, because the melts has a lot of non-bonding interactions and non-periodic structure. To investigating the methods, we have chosen solid-oxygen model which has both conditions of the crystal and molecule and measured by our corroborators [1]. It is the molecular crystal in lower pressure and loses the molecular character in high pressure. We have investigated the density functional method for the solid oxygen [2], and in present study, we run ab initio molecular dynamics (AI-MD) calculation for investigating the thermal effect onto the structure of the solid oxygen using the PIMD program [3] linked with parallel electronic structure calculation code, Quantum Espresso (QE) [4]. We performed AI-MD calculations for the epsilon phase of the solid oxygen in various temperatures and computational conditions with four-node parallel calculations in system B. We took 100,000 steps of NVT samplings after 10,000 equilibrium steps for each trajectory with 20 GPa volume. We used a minimum cell including eight oxygen molecules and PBE density functional with PAW method. The k-points was x5x3x2, and the energy cut off was 100. Ry.

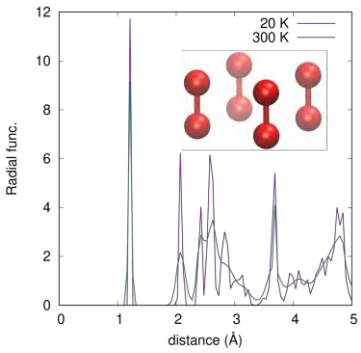

Fig. 1. Computed radial distribution function of the oxygen atoms in the ε-solid oxygen. The figure in graph is a single unit cell of the ε-oxygen.

Figure 1 shows the computed radial distribution function the ε-solid oxygen in 20 K and 300 K. The first peak is intra-molecular

distance and the second and fourth peaks are neighboring molecular distances in the unit cell. The four oxygen molecules construct a square unit and the third peak comes from the distance of next square units. Comparing 20 K and 300 K results, the position of peaks does not change while these peaks broaden. The thermal effect may conserve the structure in room temperature although we should also check the NPT sampling.

References

[1] H. Fukui et al. unpublished.

[2] L. The Anh et al. submitted.

[3] S. Ruiz-Barragan, K. Ishimura, M. Shiga: Chem. Phys. Lett., **646** (2016) 130.

[4] P. Giannozzi *et al.*: J.Phys.: Condens. Matter 21 (2009) 395502.